International Journal of Sciences: Basic and Applied Research (IJSBAR)

ISSN 2307-4531
(Print & Online)

http://gssrr.org/index.php?journal=JournalOfBasicAndApplied

In Vivo Simultaneous Imaging of Vascular Pool and Hypoxia with a HT-29 Tumor Model: The Application of Dual-Isotope SPECT/PET/CT

Naoya Adachi[a], Yukie Yoshii[b*], Takako Furukawa[c], Mitsuyoshi Yoshimoto[d], Yasuto Takeuchi [e], Masayuki Inubushi[f], Hidekatsu Wakizaka[g], Ming-Rong Zhang[h], Atsushi B Tsuji[i], Masashi Takahashi[j], Yasuhisa Fujibayashi[k], and Tsuneo Saga[l]

[a,b,c,e,g,h,I,k,l]*Molecular Imaging Center, National Institute of Radiological Sciences4-9-1 Anagawa Inage, 263-8555, Chiba, Japan*

[a,j]*Faculty of Science, Toho University, 2-2-1 Miyama, 274-8510,Funabashi, Japan*

[d]*Division of Functional Imaging, National Cancer Center Hospital East,6-5-1 Kashiwanoha, 277-8577, Kashiwa, Japan*

[e]*Institute for Genetic Medicine, Hokkaido University, Kita-15 Nishi-7 Kita-Ku, 060-0815, Sapporo, Japan*

[f]*Department of Nuclear Medicine, Kawasaki Medical School,577 Matsushima, 701-0192, Kurashiki, Japan*

[a]*Email: naoya@fml.nirs.go.jp*

[b]*Email: yukiey@nirs.go.jp*

[c]*Email: tfuru@nirs.go.jp*

[d]*Email: miyoshim@ncc.go.jp*

[e]*Email: miyoshim@ncc.go.jp*

[f]*Email: inubushi@med.kawasaki-m.ac.jp*

[g]*Email: wakisaka@nirs.go.jp*

[h]*Email: zhang@nirs.go.jp*

[i]*Email: a_tsuji@nirs.go.jp*

[j]*Email: takahasi@chem.sci.toho-u.ac.jp*

[k]*Email: yfuji@nirs.go.jp*

[l]*Email: saga@nirs.go.jp*

---

*Corresponding author .

Abstract

Investigation of vascularity and hypoxia in tumors is important in understanding cancer biology to develop the therapeutic strategies in cancer treatment. Recently, an imaging technology with the VECT or SPECT/PET/CT small-animal scanner (MILabs) has been developed to obtain simultaneous images using two different tracers labeled with SPECT and PET nuclides, respectively. In this study, we developed a method to simultaneously visualize vascularity and hypoxia with a human colon carcinoma HT-29tumor-bearing mouse model with ^{99m}Tc-labeled human serum albumin (^{99m}Tc-HSA) to detect blood pool, and ^{64}Cu-diacetyl-bis (*N*^{4}-methylthiosemicarbazone) (^{64}Cu-ATSM) to detect the over-reduced conditions under hypoxia, by applying this SPECT/PET/CT technology. Prior to the *in vivo* experiments, a phantom study was conducted to confirm quantitativity of the ^{99m}Tc/^{64}Cu dual-isotope imaging with the SPECT/PET/CT system, by comparing radio activities detected by SPECT/PET/CT system and those of standards under the conditions of wide range of radio activities and various content ratios, in our settings. An *in vivo* imaging study was conducted with HT-29 tumor-bearing mice. Both ^{64}Cu-ATSM (37 MBq) and ^{99m}Tc-HSA (18.5 MBq) were intravenously injected into a mouse (n = 4) at 1 h and 10 min, respectively, before scanning for 20 min; the ^{99m}Tc/^{64}Cu dual-isotope SPECT/PET/CT images were then obtained. The phantom study demonstrated that this system has high quantitativity, even when 2 isotopes co-existed and the content ratio was changed over a wide range, indicating the feasibility for *in vivo* experiments. *In vivo* SPECT/PET/CT imaging with ^{64}Cu-ATSM and ^{99m}Tc-HSA visualized the distribution of each probe and showed that ^{64}Cu-ATSM high-uptake regions barely overlapped with ^{99m}Tc-HSA high-uptake regions within HT-29 tumors. We developed a method to simultaneously visualize vascularity and hypoxia within HT-29tumors using *in vivo*dual-isotope SPECT/PET/CT imaging. This methodology would be useful for studies on cancer biology with mouse tumor models and development of the treatment strategies against cancer.

Examination of vascularity and hypoxia within in vivotumors is important in understanding the biology of cancer and development of the therapeutic strategies in cancer treatment. For hypervascular tumors, antiangiogenic therapy and antivascular therapy are promising approaches. For antiangiogenic therapy, the anti-vascular endothelial growth factor antibody bevacizumab is now clinically used worldwide [1-4], and for antivascular therapy, a clinical trial with combrestatin A4 phosphate is conducted [5]. For hypovascular tumor, which is usually associated with hypoxia, intensive treatment is necessary, since tumor hypoxia is reportedly resistant to chemotherapy and radiotherapy [6-8]. In recent years, several therapeutic methods have been proposedto damage to hypoxic regions within tumors, such as intensity modulated radiation therapy with hypoxia positron emission tomography (PET) imaging [9, 10], and carbon-ion radiotherapy, which is able to damage tumor cells even in the absence of oxygen by high linear energy transfer beam [11, 12]. However, considering the difficulty of cancer radical cure at the present moment, more effective drugs and treatment methods for antiangiogenic, antivascular, and antihypoxia therapies need to be developed. In addition, combinations of these therapies would be effective approaches, since they can attack tumor vascularity and hypoxia closely linked each other. However, it is still difficult to observe tumor vascularity and hypoxia both coincidently and concisely in *in vivo* tumor-bearing mouse model.

Recently, a technology of single-photon emission computed tomography/positron emission

tomography/computed tomography (SPECT/PET/CT) imaging with the VECT or small-animal scanner, launched from MILabs (Utrecht, Netherlands), has been reported to obtain truly simultaneous images with two tracers labeled with SPECT and PET nuclides, respectively. Conventionally, dual-isotope imaging studies with SPECT and PET have been performed by obtaining each image independently with 2 separate systems [13, 14]. In contrast, the VECT or system is equipped with a clustered pinhole collimator, which dramatically reduces pinhole-edge penetration of high-energy annihilation γ-photons from PET nuclides and enables it to detect high-energy γ-photons derived from PET nuclides, in a manner similar to SPECT nuclides, and to obtain high-resolution images from positron emitters and single-photon emitters at the same time by separating the images based on the photon energy [15, 16]. Thus, this system has a novel concept to make images of PET nuclides, compared to the typical PET system, which measures the coincidence of annihilation γ-photons. Goorden et al. have reported that this system shows high spatial resolution, with 0.8 mm for PET nuclides and 0.5 mm for SPECT nuclides [15]. Miwa et al. also confirmed its performance in simultaneous detection of ^{99m}Tc and ^{18}F using this system [17].

In this study, we developed a methodology to easily observe in tratumoral vascularity and hypoxia in a simultaneous manner, by applying this SPECT/PET/CT technology. We used ^{99m}Tc-labeled human serum albumin (^{99m}Tc-HSA) labeled with a SPECT nuclide ^{99m}Tc (half-life = 6.0 h; 140 keV γ-ray: 89%) to visualize tumor vascularity by detecting blood pool [18]. The ^{99m}Tc-HSAhas been reported to detect tumor blood pool in many types of cancer, including colon cancer, renal cell carcinoma, and liver tumor in both preclinical and clinical studies [19-21]. We also used ^{64}Cu-diacetyl-bis (N^4-methylthiosemicarbazone) (^{64}Cu-ATSM), labeled with a PET nuclide ^{64}Cu (half-life = 12.7 h; β^+-decay: 17.4%; β^--decay: 38.5%; and electron capture: 43%) [22], to detect tumor hypoxia. The Cu-ATSM, labeled with Cu radioisotopes, such as ^{60}Cu, ^{62}Cu, and ^{64}Cu, has been developed as an imaging agent targeting hypoxic regions in tumors for use with PET [23-26].Many studies have demonstrated that Cu-ATSM accumulation is associated with hypoxic conditions of tumor *in vitro* and *in vivo*[26-29]. The mechanism of radiolabeled Cu-ATSM accumulation has been studied: Cu-ATSM has small molecular size and high membrane permeability, and thus rapidly diffuses into cells and is reduced and trapped within cells under highly reduced intracellular conditions such as hypoxia [24, 29-31]. A clinical study with ^{62}Cu-ATSM demonstrated that high levels of hypoxia-inducible factor-1α (HIF-1α) expression were found in Cu-ATSM uptake regions in the tumors of patients with glioma [32]. In this study, we performed simultaneous *in vivo* imaging using a SPECT/PET/CT with ^{99m}Tc-HSA and ^{64}Cu-ATSM for detecting tumor vascularity and hypoxia with a HT-29 tumor-bearing mouse model.

Keywords: ^{64}Cu-ATSM; hypoxia; dual-isotope imaging; PET;SPECT; ^{99m}Tc-HSA; vascularity.

1. Materials and Methods

1.1. Preparation of radiochemical compounds

In this study, we used ^{99m}Tc as a SPECT nuclide and ^{64}Cu as a PET nuclide. The ^{99m}Tc-pertechnetate was purchased from Nihon Medi-Physics (Tokyo, Japan). The ^{64}Cu was produced in the cyclotron facility in our institution, as reported previously [33] and dissolved in 0.1 M ammonium citrate (pH: 5.5). For the phantom study, the ^{99m}Tc and the ^{64}Cu solutions were used. For the *in vivo* study, a blood pool-detecting agent (^{99m}Tc-

HSA) and a hypoxia-detecting agent (^{64}Cu-ATSM) were synthesized. For the ^{99m}Tc-HSA, we used the Techne Albumin Kit (Fujifilm RI Pharma, Tokyo, Japan), according to the manufacturer's protocol. The synthesis of ^{64}Cu-ATSM was performed as previously described [34].

1.2. SPECT/PET/CT imaging

The VECT or small-animal scanner (MILabs, Utrecht, Netherlands) with the tungsten collimator and the NaI(Tl) crystal detectors, was used for SPECT/PET/CT imaging. The mouse PET 0.7 collimator, which contains 48 clusters of four 0.7-mm diameter pinholes placed in 4 rings, and whose central field of view is approximately 12 mm in diameter and approximately 9 mm in longitudinal length [15], was used in this study. Simultaneous SPECT/PET/CT scan was performed for 20 min by list-mode acquisitions using the manufacturer's software (version 3.6g3s, MILabs). For CT, non-contrast-enhanced acquisitions were performed with the following parameters: 60 kV tube voltage, 615 μAtube current, partial scan angle, and fast scan mode. The SPECT/PET projections were reconstructed with a pixel-based, ordered-subsets expectation maximization algorithm [35] by a software attached to the VECT or (version 2.38c), and the triple-energy window method [36] was used for scatter correction with the following parameters: for ^{99m}Tc, photo peak windows was set to a width of 29%; background = 10% on left side and 7% on right side of the photo peak; 16 subset; 15 iteration; 0.4-mm voxel size; and no filter, and for ^{64}Cu, photo peak window was set to a width of 30.2%; background = 10% on left side and 7% on right side of the photo peak; 32 subset; 15 iteration; 0.4-mm voxel size; and no filter. These parameters were decided based on [15, 37]. Registration of the reconstructed SPECT, PET, and CT images was performed with the software (version 2.38c). Registered SPECT/PET/CT images were analyzed by the biomedical image quantification software PMOD (PMOD Technologies Ltd, Zürich, Switzerland). Radioactivity density values (kBq/cc) on SPECT and PET images were determined based on the calibration with a known activity concentration using the decay correction.

1.3. Phantom study

To confirm quantitativity of the ^{99m}Tc/^{64}Cu dual-isotope imaging using the VECT or SPECT/PET/CT system in our settings, a phantom study was performed under the conditions of wide range of radio activities and various content ratios. For the phantom study, cylindrical phantoms made of 1-ml syringes (Terumo, Tokyo, Japan) containing 100 μl radioactive solutions were used. In phantom study 1, we performed a comparison of quantitativity between phantoms containing mixed dual isotopes (^{99m}Tc + ^{64}Cu) and each single isotope (^{99m}Tc or ^{64}Cu). For this experiment, we prepared phantoms containing mixed dual isotopes in various concentrations with a radioactivity ratio ^{99m}Tc :^{64}Cu = 1 : 2 and each single isotope (^{99m}Tc or ^{64}Cu), as shown in Table 1.

In phantom study 2, quantitativity was examined with dual isotope (^{99m}Tc + ^{64}Cu) samples mixed at different ratios. For this experiment, ^{99m}Tc was mixed with a given amount of ^{64}Cu at various ratios in the phantoms, as seen in Table 2. Radioactivity determined with a dose calibrator (IGC-7 curiemeter; Hitachi Aloka Medical, Tokyo, Japan) was enclosed in the phantoms; this radioactivity was used as a reference standard in phantom studies 1 and 2. From the obtained SPECT and PET images, the radioactivity of the phantoms was calculated with the radioactivity density values, which were determined as described above.

1.4. In vivo ^{99m}Tc/^{64}Cu dual-isotope imaging with HT-29 tumor-bearing mouse model

Mice bearing human colon carcinoma HT-29 tumors were used in this study. The HT-29 cells (HTB-38; American Type Culture Collection, Manassas, VA) were incubated in a humidified atmosphere of 5% CO_2 in air at 37°C. We used Dulbecco's modified Eagle's medium, supplemented with 10% fetal bovine serum and antibiotics as the growth medium. Exponentially growing cells were used in this study.

Table 1: Radioactivity concentration in the phantoms used in phantom study 1

Single-isotope phantoms		
^{99m}Tc alone (kBq)	^{64}Cu alone (kBq)	Dual-isotope phantoms[^{99m}Tc (kBq) + ^{64}Cu (kBq)]
18,500	37,000	18,500 + 37,000
9,250	18,500	9,250 + 18,500
5,550	11,100	5,550 + 11,100
1,850	3,700	1,850 + 3,700
925	1,850	925 + 1,850
462.5	925	462.5 + 925
231.3	462.5	231.3 + 462.5
115.6	231.3	115.6 + 231.3
0	0	0 + 0

Table 2: Radioactivity concentration in the phantoms used in phantom study 2

	Dual-isotope phantoms	
^{99m}Tc : ^{64}Cu ratio	^{99m}Tc (kBq)	^{64}Cu (kBq)
1 : 1	1,850	1,850
0.5 : 1	925	1,850
0.25 : 1	462.5	1,850
0.125 : 1	231.3	1,850
0.0625 : 1	115.6	1,850
0 : 1	0	1,850

The incubated cells were trypsinized to detach them from the plates, and the number of cells was counted with a Cytorecon (GE Healthcare, Princeton, NJ). The BALB/c male nude mice (age: 6 weeks; body weight: 20-25 g) were purchased from Japan SLC (Shizuoka, Japan). The HT-29 cells suspended in phosphate-buffered saline (1×10^7 cells) were subcutaneously injected into the femoral region of the right hind leg of the BALB/c nude mouse. When tumors reached approximately 8 to 12 mm in diameters, in which no obvious necrotic foci were observed, the imaging study was performed (n = 4). We intravenously injected 37 MBq of ^{64}Cu-ATSM and 18.5 MBq of

^{99m}Tc-HSA into a mouse at 1 h and 10 min before the SPECT/PET scan, respectively. Injection dose and timing of these tracers were decided based on the previous studies [17, 38, 39].Each probe was dissolved in 100 µl of saline. A 20-min SPECT/PET scan, followed by CT scan, was performed, focusing on the tumor region. During the scans, the mice remained under 2% isoflurane anesthesia, and body temperature was maintained with a heater during the scans, on the attached measurement stage. With the reconstructed and registered images, the regions of interest (ROIs) were positioned on the tumor regions. The standardized uptake values (SUVs), the mean activity concentration divided by the injected activity per body weight, were calculated for each pixel in the ROIs. For the evaluation of acquired images, high-uptake regions for ^{99m}Tc and ^{64}Cu were determined with various threshold values (10%, 20%, 30%, 40%, 50%, 60%, 70%, 80%, and 90% of each SUV_{max}value in each ROI) and the percentage of overlapped areas of ^{99m}Tc and ^{64}Cu high-uptake regions in the ROIs were calculated: percentage of overlapped area = (areas of both ^{99m}Tc and ^{64}Cu high uptake in the ROI) / (all areas of the ROI) × 100. From this, the minimal threshold value, which shows little overlap of ^{99m}Tc-HSA and ^{64}Cu-ATSM high-uptake regions, was determined in the HT-29 tumor model.

1.5. Ethics statement

Animal experiments in this study were carried out in strict accordance with the recommendations in the Guide for the Care and Use of Laboratory Animals of our institution. The protocol was approved by the Animal Ethics Committee of our institution (Permit Number: M40-01). All efforts were made to minimize suffering in the animal experiments.

2. Results

2.1. Phantom studies

In phantom study 1, the radioactivity of phantoms containing mixed dual isotopes (^{99m}Tc + ^{64}Cu) and single isotopes (^{99m}Tc or ^{64}Cu), was measured by SPECT/PET/CT imaging. Figure 1 shows the representative energy spectra of ^{99m}Tc alone (Figure 1a), ^{64}Cu alone (Figure 1b), and dual isotopes (^{99m}Tc + ^{64}Cu)(Figure 1c), respectively. We observed a single main peak of ^{99m}Tc (140 keV) in the spectrum of ^{99m}Tcalone, while the spectrum of ^{64}Cu alone showed a primary photopeak (511 keV) and the broad peak, which is considered to be the backscatter of photons derived from ^{64}Cu [17]. In the spectrum of ^{99m}Tc + ^{64}Cu, the backscatter of photons derived from ^{64}Cu overlapped with the main peak of ^{99m}Tc. Since there was no peak at 511 keV in the spectrum of ^{99m}Tcalone, photons of 511 keV in dual isotopes (^{99m}Tc + ^{64}Cu) were considered to be derived from ^{64}Cu. Figure 2a shows the comparison between the ^{99m}Tcradioactivity measured by SPECT/PET/CT images and that of standard radioactivity in phantoms with dual isotopes (^{99m}Tc + ^{64}Cu) and single isotopes (^{99m}Tc alone) in the range of 0 to 18,500 kBq for ^{99m}Tc and 0 to 37,000 kBq for ^{64}Cu. The ^{99m}Tcradioactivity obtained by SPECT/PET/CT imaging was proportional to standard radioactivity, and the slope was almost 1, which were similar in both dual- and single-isotope phantoms: slope = 0.96 and R^2 = 0.99 for ^{99m}Tc in phantoms with dual isotopes (^{99m}Tc + ^{64}Cu), and slope = 1.01 and R^2 = 0.99 for ^{99m}Tc in phantoms with ^{99m}Tc alone, respectively. This result was similar in the case of ^{64}Curadioactivity in the comparison between phantoms with dual-isotopes (^{99m}Tc + ^{64}Cu) and single isotopes (^{64}Cu alone): slope = 0.96 and R^2 = 0.99 for ^{64}Cu in phantoms with dual isotopes (^{99m}Tc + ^{64}Cu), and slope = 1.05 and R^2 = 0.99 for ^{64}Cu in phantoms with ^{64}Cu alone, respectively

(Figure 2b). These data mean that radioactivity obtained by SPECT/PET/CT imaging with this method is consistent with that of standards in the range of this experiment.

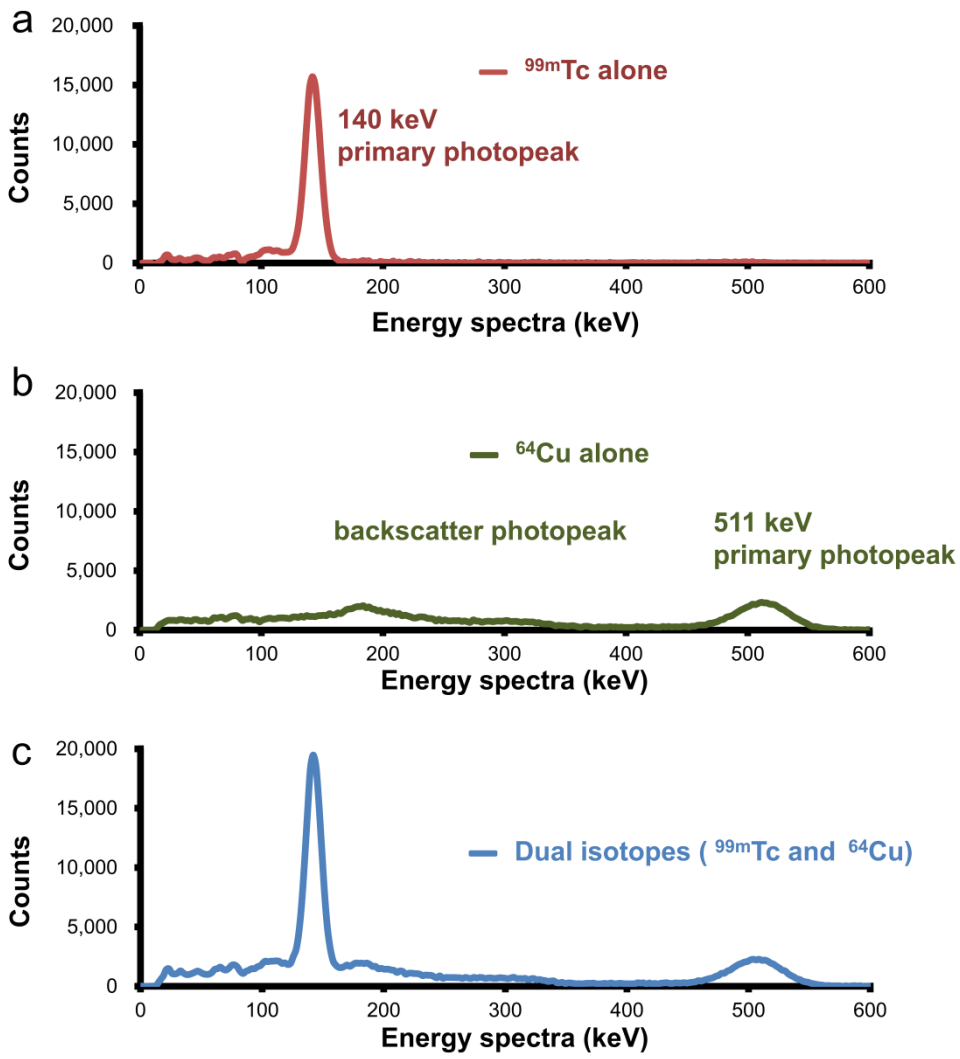

Figure 1 : Representative energy spectra measured by the SPECT/PET/CT system

The energy spectra for ^{99m}Tc alone (115.6 kBq) (a), ^{64}Cu alone (231.3 kBq) (b), and dual isotopes (^{99m}Tc + ^{64}Cu) (115.6 kBq for ^{99m}Tc, and 231.3 kBq for ^{64}Cu) (c). There was a 140-keV primary photopeak in the spectrum of ^{99m}Tcalone, a 511-keV primary photopeak (annihilation γ-photons), and a backscatter photopeak in the spectrum of ^{64}Cu alone.

(a**)**The^{99m}Tcradioactivity measured using SPECT/PET/CT (y axis) plotted against the standard radioactivity (x axis) in phantoms with single isotopes (^{99m}Tc alone) (red line) and dual isotopes (^{99m}Tc + ^{64}Cu) (blue line) in various concentrations, at a radioactivity ratio of ^{99m}Tc :^{64}Cu = 1 : 2 (see Table 1). (b) The ^{64}Curadioactivity measured by SPECT/PET/CT (y axis) plotted against the standard radioactivity (x axis) in phantoms with single isotopes (^{64}Cu alone) (green line) and dual isotopes (^{99m}Tc + ^{64}Cu) (blue line) in various concentrations, with a radioactivity ratio of ^{99m}Tc :^{64}Cu = 1 : 2 (see Table 1).

In phantom study 2, the ^{99m}Tc radioactivity of phantoms mixed with ^{99m}Tc at various ratios to a given amount of ^{64}Cu was measured with SPECT/PET/CT. In this experiment, we focused on the quantitativity at the low content of ^{99m}Tc to ^{64}Cu, since the spectra data showed that the main peak of ^{99m}Tc overlapped with the backscatter photopeak of ^{64}Cu. Figure 3 shows the comparison between ^{99m}Tc radioactivity measured by SPECT/PET/CT imaging and that of standard radioactivity (^{99m}Tc: ^{64}Cu ratio = 0, 0.0625, 0.125, 0.25, 0.5, 1: 1; ^{64}Cu radioactivity = 1850 kBq). The ^{99m}Tc radioactivity obtained by SPECT/PET/CT imaging was proportional to standard radioactivity and the slope was 0.99 (R^2 = 0.99). The ^{99m}Tc radioactivity was consistent between SPECT/PET/CT imaging and standard radioactivity, even at the lowest ^{99m}Tc: ^{64}Cu ratio (0.0625:1).

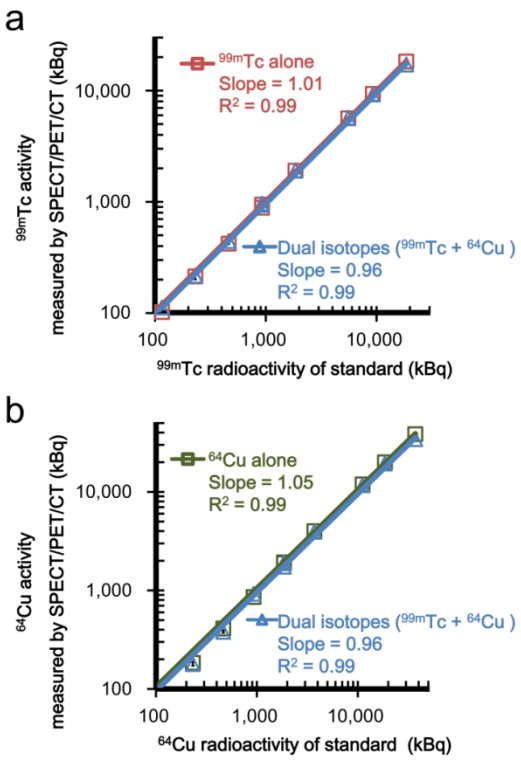

Figure 2: Comparison between radioactivity measured by SPECT/PET/CT and that of standard radioactivity in phantom study 1

2.2. In vivo ^{99m}Tc/^{64}Cu dual-isotope imaging study

Thein vivo SPECT/PET/CT imaging study was performed with HT-29 tumor-bearing mice, injected with ^{64}Cu-ATSM (37 MBq) and ^{99m}Tc-HSA (18.5 MBq). Figure 4 shows representative images of ^{99m}Tc-HSA (Figure 4a) and ^{64}Cu-ATSM (Figure 4b) by SPECT/PET/CT of a HT-29 tumor. The ^{99m}Tc-HSA uptake regions, colored red,and the ^{64}Cu-ATSM uptake regions, colored green, were barely overlapped in the merged image (Figure 4c). Figure 5a and 5b indicate the percentage of high uptake regions, determined with various threshold values, within tumors for ^{99m}Tc and ^{64}Cu, and Figure 5c shows the percentage of overlapped areas of high-uptake regions from 2 tracers within the tumor, when various thresholds for both ^{99m}Tc and ^{64}Cu in common were employed. The percentage of overlapped area was dramatically reduced, from 2.9% ± 0.9 at 30% threshold value to negligible (0.6% ± 0.3%) at 40% threshold value. This means ^{99m}Tc-HSA and ^{64}Cu-ATSM high-uptake regions are little

overlapped when the threshold value was set to be 40% or higher of SUV_{max}, for both probes. Taken together, our data demonstrated that high-uptake regions of ^{99m}Tc-HSA and ^{64}Cu-ATSM were clearly distinguished within tumors with this method using dual-isotope SPECT/PET/CT imaging.

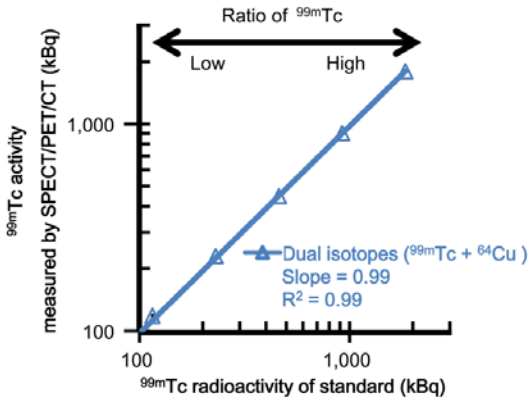

Figure 3: Comparison between radioactivity measured by SPECT/PET/CT and that of standard radioactivity in phantom study 2

The ^{99m}Tc radioactivity measured by SPECT/PET/CT (y axis) plotted against the standard ^{99m}Tc radioactivity (x axis) in phantoms with ^{99m}Tc mixed at various ratios, to a given amount of ^{64}Cu (see Table 2).

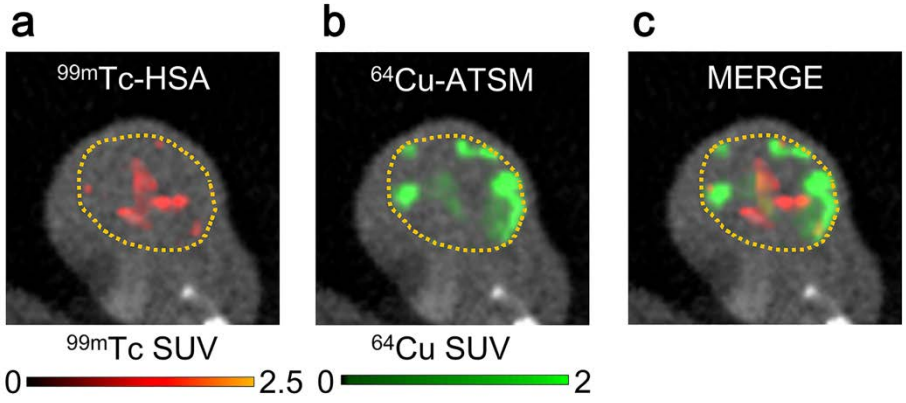

Figure 4: In vivoSPECT/PET/CT imaging with ^{99m}Tc-HSA and ^{64}Cu-ATSM

Representative images of HT-29 tumor-bearing miceinjected with 18.5 MBq of ^{99m}Tc-HSA and 37 MBq of ^{64}Cu-ATSM are shown: ^{99m}Tc-HSA (a), ^{64}Cu-ATSM (b), and merged ^{99m}Tc-HSA and ^{64}Cu-ATSM (c). Dotted yellow circles indicate tumor regions in a through c. Red indicates ^{99m}Tc-HSA uptake in a and c, and green, ^{64}Cu-ATSM uptake in b and c.

The percentage of high-uptake regions of ^{99m}Tc-HSA (a) and ^{64}Cu-ATSM (b) in tumors with various threshold values of $\%SUV_{max}$ for each probe are shown, as well as the percentage of overlapped areas between high-uptake regions for ^{99m}Tc-HSA and ^{64}Cu-ATSM in tumors, with various thresholds of $\%SUV_{max}$ for both probes

in common (c). Values are shown as mean ± SD (n = 4).

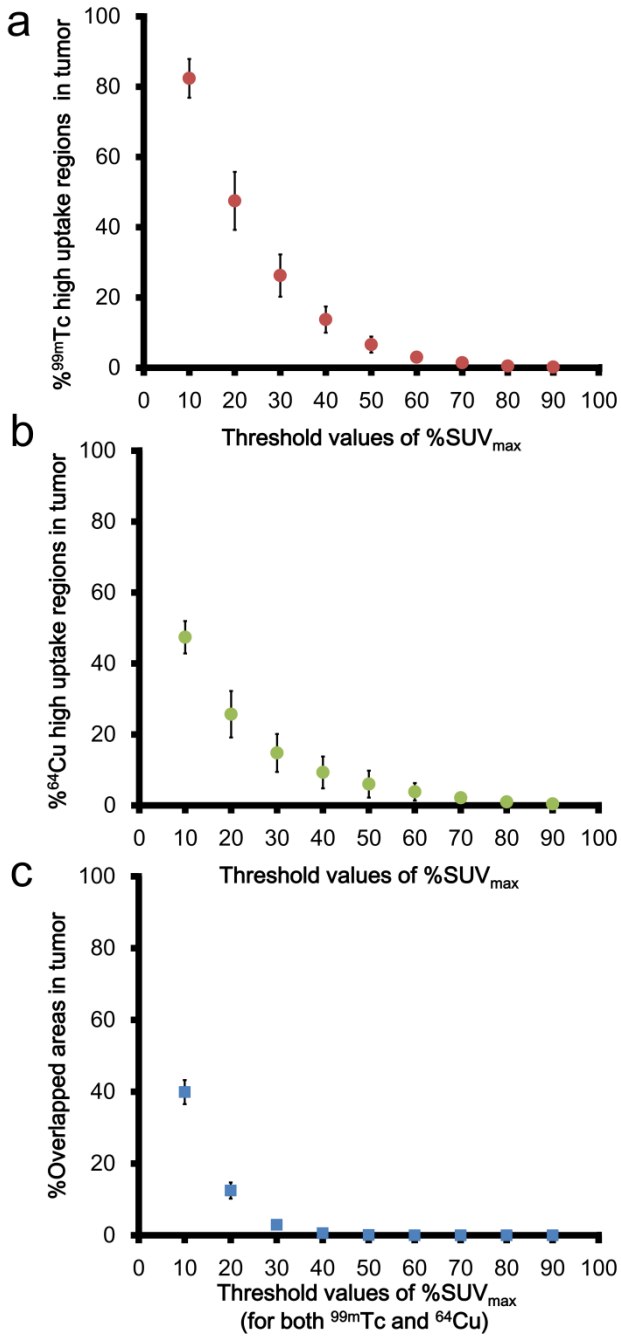

Figure5: Analysis of the overlap between *in vivo* SPECT/PET/CT images of ^{99m}Tc-HSA and ^{64}Cu-ATSM in HT-29 tumors

3. Discussion

Phantom study 1 demonstrated that ^{99m}Tc/^{64}Cu SPECT/PET/CT showed high quantitativity, even when 2 isotopes co-existed, in the range of 0 to 18,500 kBq for ^{99m}Tc and 0 to 37,000 kBq for ^{64}Cu, which seems to be wide enough to cover the range of radioactivity expected in *in vivo* experiments in mice. Phantom study 2

demonstrated that the quantitativity of ^{99m}Tc/^{64}Cu SPECT/PET/CT remained high even when the content ratios of ^{99m}Tc and ^{64}Cu were changed. These experiments demonstrated that the cross-talk effect of the backscatter of photons derived from ^{64}Cu overlapped with the main peak of ^{99m}Tc (140 keV) was minimal in this method, in the wide range of radioactivity and even at the low content of ^{99m}Tc to ^{64}Cu. From our phantom studies, we confirmed that ^{99m}Tc/^{64}Cu dual-isotope SPECT/PET/CT imaging would be feasible for *in vivo* experiments.

Our in vivo study demonstrated that dual-isotope SPECT/PET/CT imaging can simultaneously visualize tumor vascularity detected by ^{99m}Tc-HSA and hypoxia detected by ^{64}Cu-ATSM in a human colon carcinoma HT-29tumor-bearing mouse model. Our data showed that overlapped areas between ^{99m}Tc-HSA and ^{64}Cu-ATSM high-uptake regions, defined using the threshold value as 40% or higher of SUV_{max} within tumors, were very limited. Previously, many in vitro and in vivo studies have demonstrated that ^{64}Cu-ATSM uptake is related to hypoxia within tumors [26-29]; it has been reported that ^{64}Cu-ATSM high-uptake regions within tumors are hypovascular, undergoing cell cycle arrest but little necrosis, while ^{64}Cu-ATSMlow-uptake regions are hypervascular, showing active cell proliferation [40, 41]. Also, previous preclinical and clinical studies have shown that ^{99m}Tc-HSA can detect tumor blood pool [19-21]. Considering this evidence, the observations in this study, which show little overlap between ^{99m}Tc-HSA and ^{64}Cu-ATSM high-uptake regions, seem reasonable. The ^{64}Cu-ATSM autoradiography analyses in the previous preclinical studies have reported the distribution pattern of that the ^{64}Cu-ATSM high-uptake regions associated with hypovascularity are located in the peripheral regions and the ^{64}Cu-ATSM low-uptake regions associated with hypervascularity are located in the central regions within tumors, in several types of tumor-bearing mouse models including HT-29 [40, 42], which is a similar result to the present study with SPECT/PET/CT imaging. Since this probe has small molecular size and high membrane permeability [24] and the previous preclinical and clinical studies demonstrated that Cu-ATSM can reach to the central part in tumors [42, 43], the low of accumulation of ^{64}Cu-ATSM in the central regions of HT-29 tumor model is considered not due to the low penetration.

Our data demonstrated that dual-isotope SPECT/PET/CT with ^{99m}Tc-HSA and ^{64}Cu-ATSM can simultaneously visualize vascularity and hypoxia within HT-29 tumors in mice. This methodology would have a potential to be applied to the other tumor-bearing mouse models. The method developed in this study enables coincident and precise observations of vascularity and hypoxia in vivo, which could help to understand the dynamics of tumor micro enviroments related to vascularity and hypoxia. In addition, this method could contribute to the development of new drugs and treatment strategies for antiangiogenic, antivascular, and antihypoxia therapy.

4. Conclusion

In conclusion, we developed a dual-isotope SPECT/PET/CT imaging with ^{99m}Tc-HSA and ^{64}Cu-ATSM to simultaneously visualize vascularity and hypoxia with a HT-29 tumor-bearing mouse model. This could be useful for understanding tumor microenvironment and development.

Acknowledgements

We would like to thank Mr. Hisashi Suzuki (National Institute of Radiological Sciences, Chiba, Japan) for

providing the radiopharmaceuticals. This work was supported by Grants-in-Aid from The Uehara Memorial Foundation, Tokyo, Japan.

References

[1].Kuroda J, Kuratsu J, Yasunaga M, Koga Y, Kenmotsu H, Sugino T, et al. "Antitumor effect of NK012, a 7-ethyl-10-hydroxycamptothecin-incorporating polymeric micelle, on U87MG orthotopicglioblastoma in mice compared with irinotecan hydrochloride in combination with bevacizumab."Clin Cancer Res. 2010;16(2):521-9.

[2].Mukherji SK. "Bevacizumab (Avastin)."AJNR Am J Neuroradiol. 2010;31(2):235-6.

[3].Leu K, Enzmann DR, Woodworth DC, Harris RJ, Tran AN, Lai A, et al. "Hypervascular tumor volume estimated by comparison to a large-scale cerebral blood volume radiographic atlas predicts survival in recurrent glioblastoma treated with bevacizumab."Cancer Imaging. 2014;14:31, Available:www.cancerimagingjournal.com/content/14/1/31[Dec.11,2015].

[4].Jennings D, Raghunand N, Gillies RJ. "Imaging hemodynamics."Cancer Metastasis Rev. 2008;27(4):589-613.

[5].Rustin GJ, Galbraith SM, Anderson H, Stratford M, Folkes LK, Sena L, et al. "Phase I clinical trial of weekly combretastatin A4 phosphate: clinical and pharmacokinetic results."J ClinOncol. 2003;21(15):2815-22.

[6].Brown JM. "The hypoxic cell: a target for selective cancer therapy--eighteenth Bruce F. Cain Memorial Award lecture."Cancer Res. 1999;59(23):5863-70.

[7].Phillips RM, Loadman PM, Cronin BP. "Evaluation of a novel in vitro assay for assessing drug penetration into avascular regions of tumours."Br J Cancer. 1998;77(12):2112-9.

[8].Höckel M, Vaupel P. "Tumor hypoxia: definitions and current clinical, biologic, and molecular aspects."J Natl Cancer Inst. 2001;93(4):266-76.

[9].Chao KSC, Bosch WR, Mutic S, Lewis JS, Dehdashti F, Mintun MA, et al. "A novel approach to overcome hypoxic tumor resistance: Cu-ATSM-guided intensity-modulated radiation therapy."Int J RadiatOncolBiol Phys. 2001;49(2):1171–82.

[10]. Hendrickson K, Phillips M, Smith W, Peterson L, Krohn K, Rajendran J. "Hypoxia imaging with [F-18] FMISO-PET in head and neck cancer: potential for guiding intensity modulated radiation therapy in overcoming hypoxia-induced treatment resistance."RadiotherOncol. 2011;101(3):369-75.

[11]. Nakano T, Suzuki Y, Ohno T, Kato S, Suzuki M, Morita S, et al. "Carbon beam therapy overcomes the radiation resistance of uterine cervical cancer originating from hypoxia."Clin Cancer Res. 2006;12(7):2185-90.

[12]. Furusawa Y, Fukutsu K, Aoki M, Itsukaichi H, Eguchi-Kasai K, Ohara H, et al. "Inactivation of aerobic and hypoxic cells from three different cell lines by accelerated ^{3}He-, ^{12}C- and ^{20}Ne-ion beams". Radiat Res. 2000;154(5):485-96.

[13]. Lu Y, Yang K, Zhou K, Pang B, Wang G, Ding Y, et al. "An integrated quad-modality molecular imaging system for small animals." J Nucl Med. 2014;55(8):1375-9.

[14]. Magota K, Kubo N, Kuge Y, Nishijima K-i, Zhao S, Tamaki N. "Performance characterization of the Inveon preclinical small-animal PET/SPECT/CT system for multimodality imaging."Eur J Nucl Med Mol Imaging. 2011;38(4):742-52.

[15]. Goorden MC, Have Fvd, Kreuger R, Ramakers RM, Vastenhouw B, Burbach JPH, et al. "VECTor: a

preclinical imaging system for simultaneous submillimeter SPECT and PET." J Nucl Med. 2013;54(2):306-12.

[16]. Walker MD, Goorden MC, Dinelle K, Ramakers RM, Blinder S, Shirmohammad M, et al. "Performance assessment of a preclinical PET scanner with pinhole collimation by comparison to a coincidence-based small-animal PET scanner."J Nucl Med. 2014;55(8):1368-74.

[17]. Miwa K, Inubushi M, Takeuchi Y, Katafuchi T, Koizumi M, Saga T, et al. "Performance characteristics of a novel clustered multi-pinhole technology for simultaneous high-resolution SPECT/PET."Ann Nucl Med. 2015;29(5):460-6.

[18]. Schmitt A, Bernhardt P, Nilsson O, Ahlman H, Kölby L, Forssell-Aronsson E. "Differences in biodistribution between ^{99m}Tc-depreotide, ^{111}In-DTPA-octreotide, and ^{177}Lu-DOTA-Tyr^{3}-octreotate in a small cell lung cancer animal model."Cancer BiotherRadiopharm. 2005;20(2):231-6.

[19]. Welt S, Divgi CR, Real FX, Yeh SD, Garin-Chesa P, Finstad CL, et al. "Quantitative analysis of antibody localization in human metastatic colon cancer: a phase I study of monoclonal antibody A33."J ClinOncol. 1990;8(11):1894-906.

[20]. Oosterwijk E, Bander NH, Divgi CR, Welt S, Wakka JC, Finn RD, et al. "Antibody localization in human renal cell carcinoma: a phase I study of monoclonal antibody G250."J ClinOncol. 1993;11(4):738-50.

[21]. Levin VA, Freeman-Dove M, Landahl HD. "Permeability characteristics of brain adjacent to tumors in rats."Arch Neurol. 1975;32(12):785-91.

[22]. Lewis JS, Laforest R, Dehdashti F, Grigsby PW, Welch MJ, Siegel BA. "An imaging comparison of ^{64}Cu-ATSM and ^{60}Cu-ATSM in cancer of the uterine cervix."J Nucl Med. 2008;49(7):1177-82.

[23]. Dehdashti F, Grigsby PW, Lewis JS, Laforest R, Siegel BA, Welch MJ. "Assessing tumor hypoxia in cervical cancer by PET with ^{60}Cu-labeled diacetyl-bis(N^{4}-methylthiosemicarbazone)."J Nucl Med. 2008;49(2):201-5.

[24]. Fujibayashi Y, Taniuchi H, Yonekura Y, Ohtani H, Konishi J, Yokoyama A. "Copper-62-ATSM: a new hypoxia imaging agent with high membrane permeability and low redox potential."J Nucl Med. 1997;38(7):1155-60.

[25]. Lewis J, Laforest R, Buettner T, Song S, Fujibayashi Y, Connett J, et al. "Copper-64-diacetyl-bis(N^{4}-methylthiosemicarbazone): an agent for radiotherapy."ProcNatlAcadSci U S A. 2001;98(3):1206-11.

[26]. Lewis JS, McCarthy DW, McCarthy TJ, Fujibayashi Y, Welch MJ. "Evaluation of ^{64}Cu-ATSM in vitro and in vivo in a hypoxic tumor model."J Nucl Med. 1999;40(1):177-83.

[27]. Burgman P, O'Donoghue JA, Lewis JS, Welch MJ, Humm JL, Ling CC. "Cell line-dependent differences in uptake and retention of the hypoxia-selective nuclear imaging agent Cu-ATSM."Nucl Med Biol. 2005;32(6):623-30.

[28]. Lewis JS, Sharp TL, Laforest R, Fujibayashi Y, Welch MJ. "Tumor uptake of copper-diacetyl-bis(N^{4}-methylthiosemicarbazone): effect of changes in tissue oxygenation."J Nucl Med. 2001;42(4):655-61.

[29]. Obata A, Yoshimi E, Waki A, Lewis JS, Oyama N, Welch MJ, et al. "Retention mechanism of hypoxia selective nuclear imaging/radiotherapeutic agent cu-diacetyl-bis(N^{4}-methylthiosemicarbazone) (Cu-ATSM) in tumor cells."Ann Nucl Med. 2001;15(6):499-504.

[30]. Dearling JL, Lewis JS, Mullen GE, Welch MJ, Blower PJ. "Copper bis(thiosemicarbazone) complexes as hypoxia imaging agents: structure-activity relationships." J BiolInorg Chem. 2002;7(3):249-59.

[31]. Yoshii Y, Yoneda M, Ikawa M, Furukawa T, Kiyono Y, Mori T, et al. "Radiolabeled Cu-ATSM as a novel indicator of overreduced intracellular state due to mitochondrial dysfunction: studies with mitochondrial DNA-less ρ^0 cells and cybrids carrying MELAS mitochondrial DNA mutation."Nucl Med Biol. 2012;39(2):177-85.

[32]. Tateishi K, Tateishi U, Sato M, Yamanaka S, Kanno H, Murata H, et al. "Application of ^{62}Cu-diacetyl-bis (N^4-methylthiosemicarbazone) PET imaging to predict highly malignant tumor grades and hypoxia-inducible factor-1α expression in patients with glioma." AJNR Am J Neuroradiol. 2013;34(1):92-9.

[33]. Obata A, Kasamatsu S, McCarthy DW, Welch MJ, Saji H, Yonekura Y, et al. "Production of therapeutic quantities of ^{64}Cu using a 12 MeV cyclotron."Nucl Med Biol. 2003;30(5):535-9.

[34]. Yoshii Y, Furukawa T, Kiyono Y, Watanabe R, Waki A, Mori T, et al. "Copper-64-diacetyl-bis (N^4-methylthiosemicarbazone) accumulates in rich regions of $CD133^+$ highly tumorigenic cells in mouse colon carcinoma."Nucl Med Biol. 2010;37(4):395-404.

[35]. Branderhorst W, Vastenhouw B, Beekman FJ. "Pixel-based subsets for rapid multi-pinhole SPECT reconstruction."Phys Med Biol. 2010(7);55:2023-34.

[36]. Ogawa K, Harata Y, Ichihara T, Kubo A, Hashimoto S. "A practical method for position-dependent Compton-scatter correction in single photon emission CT."IEEE Trans Med Imaging. 1991;10(3):408-12.

[37]. Yang J-T, Yamamoto K,Sadato N,Tsuchida T, Takahashi N, Hayashi N, et al. "Clinical value of triple-energy window scatter correction in simultane dual-isotope single-photon emission tomography with ^{123}I-BMIPP and ^{201}TI."Eur J Nucl Med. 1997;24(9):1099-106.

[38]. Zinn KR, Douglas JT, Smyth CA, Liu HG, Wu Q,Krasnykh VN, et al. "Imaging and tissue biodistribution of ^{99m}Tc-labeled adenovirus knob (serotype 5)."Gene Ther. 1998;5(6):798-808.

[39]. Yoshii Y, Matsumoto H, Yoshimoto M, Furukawa T,Morokoshi Y,Sogawa C, et al. "Controlled administration of penicillamine reduces radiation exposure in critical organs during ^{64}Cu-ATSM internal radiotherapy: a novel strategy for liver protection."PloS one. 2014;9(1), Available:journals.plos.org/plosone/article?id=10.1371/journal.pone.0086996 [Dec.11,2015].

[40]. Tanaka T, Furukawa T, Fujieda S, Kasamatsu S, Yonekura Y, Fujibayashi Y. "Double-tracer autoradiography with Cu-ATSM/FDG and immunohistochemical interpretation in four different mouse implanted tumor models."Nucl Med Biol. 2006;33(6):743-50.

[41]. Oh M, Tanaka T, Kobayashi M, Furukawa T, Mori T, Kudo T, et al. "Radio-copper-labeled Cu-ATSM: an indicator of quiescent but clonogenic cells under mild hypoxia in a Lewis lung carcinoma model."Nucl Med Biol. 2009;36(4):419-26.

[42]. Furukawa T, Yuan Q, Jin ZH,Aung W, Yoshii Y, Hasegawa S, et al. "A limited overlap between intratumoral distribution of 1-(5-fluoro-5-deoxy-alpha-D-arabinofuranosyl)-2-nitroimidazole and copper-diacetyl-bis[N(4)-methylthiosemicarbazone]."Oncol Rep. 2015;34(3):1379-87.

[43]. Lohith TG,Kudo T,Demura Y,Umeda Y,Kiyono Y, Fujibayashi Y, et al. "Pathophysiologic correlation between ^{62}Cu-ATSM and ^{18}F-FDG in lung cancer."J Nucl Med. 2009;50(12):1948-53.